

The influence of magnetic and physiological behaviour on the effectiveness of iron oxide nanoparticles for hyperthermia

C L Dennis^{1,8}, A J Jackson^{2,3}, J A Borchers², R Ivkov⁴, A R Foreman⁴,
P J Hoopes⁵, R Strawbridge⁵, Z Pierce⁵, E Goertzig⁶, J W Lau¹ and C Gruettner⁷

¹ Materials Science and Engineering Laboratory, NIST, Gaithersburg, MD 20899-8552, USA

² NIST Center for Neutron Research, Gaithersburg, MD 20899-6102, USA

³ Department of Materials Science and Engineering, University of Maryland, College Park, MD 20742, USA

⁴ Triton BioSystems, Inc., Chelmsford, MA 01824, USA

⁵ Dartmouth College, Hanover, NH 03755, USA

⁶ Fraunhofer Institut Angewandte Polymerforschung, 14476 Potsdam-Golm, Germany

⁷ Micromod Partikeltechnologie GmbH, 18119 Rostock-Warnemuende, Germany

Received 30 November 2007, in final form 27 February 2008

Published 19 June 2008

Online at stacks.iop.org/JPhysD/41/134020

Abstract

Magnetic nanoparticles are being developed for a wide range of biomedical applications. In particular, hyperthermia involves heating the magnetic nanoparticles through exposure to an alternating magnetic field. These materials offer the potential to selectively treat cancer by heating cancer tissue locally and at the cellular level. This may be a successful method if there are enough particles in a tumor possessing a sufficiently high specific absorption rate (SAR) to deposit heat quickly while minimizing thermal damage to surrounding tissue. High SAR magnetic nanoparticles have been developed and used in mouse models of cancer. The magnetic nanoparticles comprise iron oxide magnetic cores (mean core diameter of 50 nm) surrounded by a dextran layer shell for colloidal stability. In comparing two similar systems, the saturation magnetization is found to play a crucial role in determining the SAR, but is not the only factor of importance. (A difference in saturation magnetization of a factor of 1.5 yields a difference in SAR of a factor of 2.5 at 1080 Oe and 150 kHz.) Variations in the interactions due to differences in the dextran layer, as determined through neutron scattering, also play a role in the SAR. Once these nanoparticles are introduced into the tumor, their efficacy, with respect to tumor growth, is determined by the location of the nanoparticles within or near the tumor cells and the association of the nanoparticles with the delivered alternating magnetic field (AMF). This association (nanoparticle SAR and AMF) determines the amount of heat generated. In our setting, the heat generated and the time of heating (thermal dose) provides a tumor gross treatment response which correlates closely with that of conventional (non-nanoparticle) hyperthermia. This being said, it appears specific aspects of the nanoparticle hyperthermia cytopathology mechanism may be very different from that observed in conventional cancer treatment hyperthermia.

(Some figures in this article are in colour only in the electronic version)

1. Introduction

The biological processes in cells, including cancer, are particularly susceptible to changes in temperature. In fact, a

change in temperature of 6 °C, from 37 to 43 °C, is sufficient to kill a cancer cell provided the cell is exposed to this temperature for a sufficient period of time [1, 2]. Furthermore, tissues heated to above 46 °C undergo extensive necrosis known as thermoablation. While the biology of thermal damage is well understood, this knowledge has translated poorly into clinical

⁸ Author to whom any correspondence should be addressed.

application for cancer therapy, although some success has been achieved for classic hyperthermia [3–6] (temperatures less than 46 °C) and thermoablative [7, 8] treatment. One reason is the absence of technology that effectively localizes heat to the tumor without heating surrounding healthy tissues [9]. A second limitation is the inability to accurately measure the heat dose deposited into the tumor relative to surrounding tissue [10, 11]. One technology being developed to address these limitations is the activation of susceptor materials such as magnetic iron oxide nanoparticles by excitation with an external AMF. However, the lack of information on which characteristics are important for delivering the maximum heat dose per gram of injected material [12, 13] and a full understanding of the mechanism of heat damage and the physiological effects on the heat dissipation are significant issues. This paper addresses these issues by comparing two nanoparticle samples physically, magnetically and thermally, followed by a preliminary assessment of the effect of iron oxide nanoparticle hyperthermia in mouse mammary tumors.

2. Experimental methods

The system studied here is based on iron oxide magnetic cores that are coated with dextran to form a shell, and have a diameter of less than 50 nm. The samples were synthesized by high-pressure homogenization according to the core/shell method, as outlined previously [14]. Two different sample batches were studied here. Although these two systems should be nominally identical in their cores, the dextran layer itself varies: Lot 1380684W 8 h (80684W 8 h) was coated with dextran once yielding a single dextran layer while Lot 01350684G (50684G) was coated twice for a double dextran layer.

A variety of analytical techniques have been applied to physically characterize these two systems. Analytical ultracentrifugation (AUC) was used to determine a density for the nanoparticles and an accurate size and size distribution for the iron oxide core. Photon correlation spectroscopy (PCS) was used to determine an average size and size distribution of the entire core/shell structure. The hysteresis loops were measured with a MPMS SQUID Magnetometer from Quantum Design⁹. All the measurements were made at room temperature (298 K) using a Kel-F liquid capsule holder from LakeShore Cryotronics⁹ to hold the colloid, and the field range was from $\pm 3.98 \text{ MA m}^{-1}$ ($\pm 50\,000 \text{ Oe}$). Transmission electron microscopy (TEM) was performed on a JEOL JEM3010 TEM⁹ at 300 keV. The colloids were diluted to 1/100 by volume and then dropped onto a carbon coated TEM grid to dry.

The small angle neutron scattering (SANS) experiments were conducted at the NG-3 beam line at the NIST Center for Neutron Research (NCNR) using neutrons with a wavelength of 8.4 Å. Data were collected in transmission mode with a two-dimensional detector at three different sample-to-detector

⁹ We identify certain commercial equipment, instruments, or materials in this article to specify adequately the experimental procedure. In no case does such identification imply recommendation or endorsement by the National Institute of Standards and Technology, nor does it imply that the materials or equipment identified are necessarily the best available for the purpose.

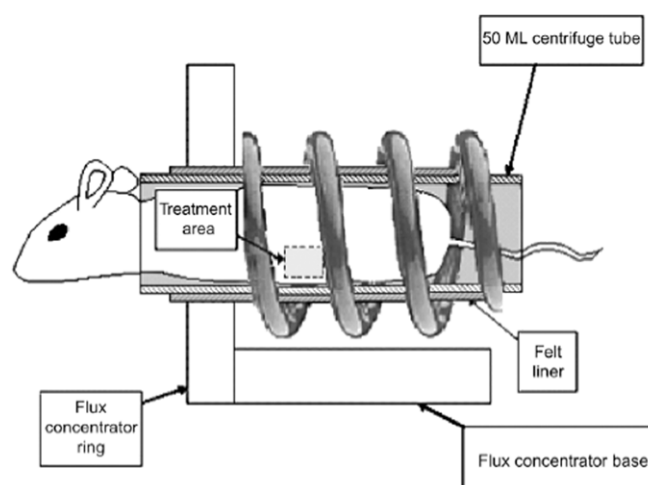


Figure 1. Schematic of the AMF set-up for the *in vivo* mouse trials.

distances, in order to span the range of scattering vectors Q from 3×10^{-5} to $5 \times 10^{-1} \text{ \AA}^{-1}$. The data were corrected for the background from an empty cell and for distortions in the detector. To probe smaller Q values, Ultra-SANS (USANS) experiments were performed using the BT-5 thermal neutron double-crystal instrument at NCNR [15]. The samples were run for 8 h each at a neutron wavelength of 2.4 Å. A background from an empty beam run was subtracted from all the data, and the subtracted data processed to an absolute scale by the use of the straight through beam intensities. The Q (wave vector component in the horizontal plane) range corresponds to probing length scales from 500 to 20 000 nm. All the SANS and USANS measurements were made at room temperature and in zero field. The samples in H₂O were held in 1 mm thick quartz cells while the samples in D₂O were held in 4 mm thick quartz cells. A series of concentrations (not shown due to space considerations) were also used in order to help constrain the parameters for the fitting. A core-shell model was used to fit the data. All SANS and USANS reduction and fits were performed using interactive IGOR procedures [16].

Specific absorption rate (SAR) measurements, to determine the heat dose of the nanoparticles, were made in a modified AMF calorimeter under varying field amplitudes at a frequency of 150 kHz. SAR values were calculated from the rate of temperature rise measured in the water when the particle suspension was heated by the AMF generated in a solenoid coil, after correction for the thermal properties of the calorimeter, coil and water. The values were normalized for iron content.

The *in vivo* mouse trials were performed in an AMF inductor [17] that confines high-amplitude magnetic fields to a 1 cm wide band of the interior of a 3.5 cm internal diameter induction coil (see figure 1). Mice were subjected to varying combinations of AMF by adjusting amplitude and duration of exposure. (The duty cycle was 100%—always on—and the frequency is fixed at 150 kHz.) The duration of exposure was limited to 15 min or when the rectal temperature of the mouse reached 41.5 °C. (This was necessary to prevent unnecessary mortality in the mice due to exposure to excessively high temperatures.) The nanoparticles were

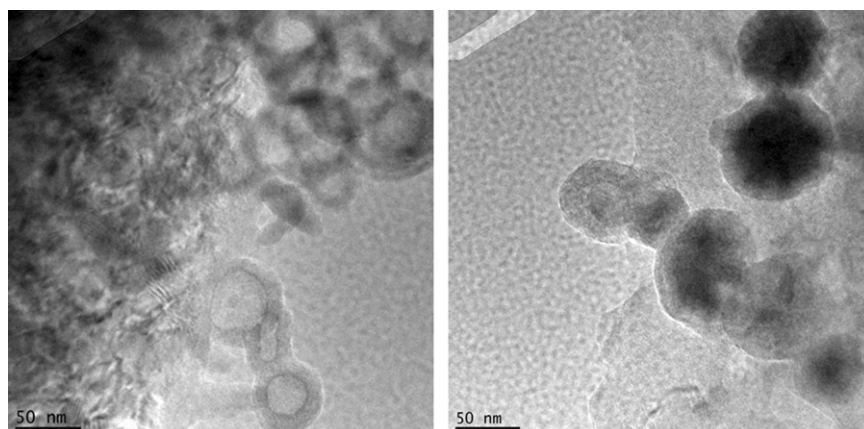


Figure 2. TEM of samples 50684G (left) and 80684W 8 h (right). Note the presence of a dark ring at the edge of the core in the 50684G sample which is not present in the 80684W 8 h sample.

directly injected into the central portion of the tumors over a 5 min period. Temperatures were continuously recorded using 0.4 mm diameter fibre optic temperature assessment probes which are not RF-sensitive and were placed in the centre of the tumor, immediately adjacent to the tumor and in the rectum.

3. Results and discussion

AUC yielded a density of 3.20 g cm^{-3} , which is slightly less than that of bulk iron oxide at 5.18 g cm^{-3} , and a size distribution of $44 \pm 13 \text{ nm}$ for the nanoparticle core. PCS yielded a larger size and size distribution of $96.5 \pm 32.4 \text{ nm}$. This number is the same whether it is determined by intensity or by volume. However, the PCS instrument estimates a hydrodynamic radius based upon a Stokes–Einstein sphere moving through the solvent and thus includes an estimate of the thickness of the dextran layer infiltrated with solvent. A dextran length of 26 nm is reasonable for the 40 000 Dalton dextran used. The AUC data also agree with the TEM images (see figure 2) that show a core diameter of $\sim 50 \text{ nm}$. The dextran layer thickness cannot be determined from the TEM as (a) it is a dried sample and (b) it is difficult to separate the amorphous dextran from the amorphous carbon film coating the TEM grid at this excitation energy. Close examination of the TEM images reveals the presence of a dark ring at the edge of the iron oxide core in the 50684G sample. This ring is not present in the 80684W 8 h sample; instead the core is denser than the edge, as expected for a sphere. This dark ring in the 50684G sample can only be due to one of two things: either the nanoparticles are thicker at the edge than in the centre or the edge has a different density than the core. The former is physically impossible for a sphere-like particle; the latter is most likely given that the density of the iron oxide is only about 62% that of the bulk. The compositional or structural origin of a density change is currently under investigation. This TEM is the first physical indication that the nanoparticle cores are actually different.

The SANS/USANS data are also in reasonable agreement with the TEM. The data for both 50684G and 80684W 8 h under different contrast conditions are shown in figure 3.

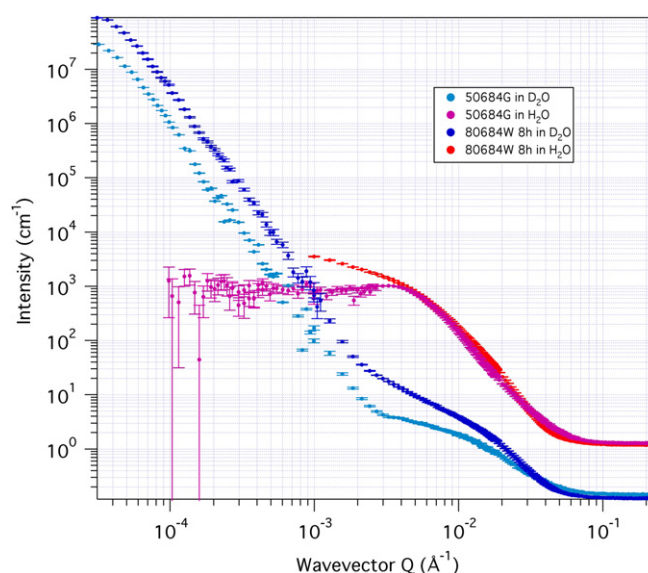


Figure 3. SANS/USANS data on the 50684G and 80684W 8 h samples in two contrasts. The D_2O data highlight both the iron oxide core (the ‘hump’ around $Q=1 \times 10^{-2}$) and the dextran (the slope for $Q < 1 \times 10^{-3}$). The H_2O data highlight just the iron oxide core. The error bars indicate ± 1 standard deviation.

H_2O and D_2O each highlight different features of the system by varying the sample contrast. In the case of H_2O the scattering is dominated by the large contrast between iron oxide and H_2O , whereas there is less contrast with dextran. In D_2O the intensity of scattering from the core is much reduced while the contrast with dextran is enhanced. Both of these samples in D_2O show a strong scattering intensity at low Q that may be due to the presence of a dextran network acting to bind particles in large-scale aggregates¹⁰. This interpretation agrees with other observations of dextran solutions [18]. However, the D_2O SANS data also highlight the

¹⁰ The extended length scales observed in SANS/USANS are not seen in the PCS data because the sample concentration in the PCS sample and the SANS/USANS/SAR sample differ by about two orders of magnitude ($0.12 \text{ mg Fe ml}^{-1}$ versus $\sim 13.4 \text{ mg Fe ml}^{-1}$). This difference is due to practical measurement considerations, although the SANS/USANS/SAR sample concentration is the same as that used in the *in vivo* mouse trials.

significant differences between the two cores. A polydisperse core-shell form-factor model was combined with a hard-sphere structure-factor model to fit the H₂O data. This yields a total particle diameter of 28.30 ± 0.02 nm. This is smaller than the size seen by either PCS or AUC, and this difference is attributed to the fact that neutron scattering is sensitive to the first moment of the distribution of radii in a polydispersed system, whereas PCS and AUC are sensitive to the third moment. Furthermore, it is possible that the radial density profile of the particles is not simply a uniform core and shell—as seen from the TEM. In addition, it is expected that there exists a decreasing density gradient of dextran with increasing radius.

The magnetic properties of the system were characterized by measuring the hysteresis loops at room temperature. These loops (see figure 4) have been normalized to the mass of particles present in the colloid using the mass of solution added to the liquid capsule holder, its density (as determined with an Anton Paar DMA 5000 Densitometer⁹), and mass concentration of material in the colloid (as determined by freeze-drying 1 ml of colloid). The most prominent point is that the saturation magnetization of the 50684G sample is 41.08 ± 0.03 kA m² g⁻¹, 33% less than that of the 80684W 8 h sample which is 61.64 ± 0.03 kA m² g⁻¹. This significant difference in magnitude may be related to the darker ring seen in the TEM. This magnetic difference further confirms that the nanoparticle cores are different.

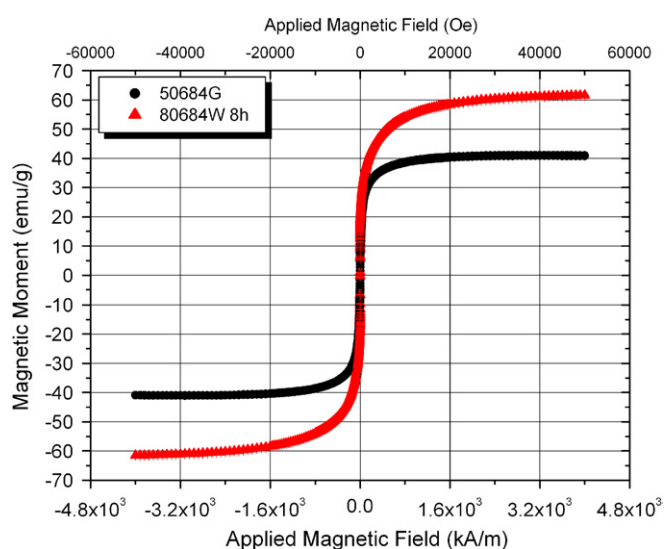


Figure 4. Hysteresis loop at 298 K of the 50684G and 80684W 8 h samples, normalized to mass of iron oxide.

The SAR values were measured for $H = 85.9$ kA m⁻¹ (1080 Oe) and $f = 150$ kHz and are normalized to iron concentration. (The 50684G sample had a colloidal concentration of 5 mg ml⁻¹ while the 80684W 8 h sample had a slightly higher concentration of 5.5 mg ml⁻¹.) The 50684G sample has a measured SAR of 209 W/(g of Fe) while the 80684 W 8 h has a measured SAR of 537 W/(g of Fe)—a difference of a factor of 2.5. Most of this difference can be attributed to the difference in the saturation magnetization, although not all. Additional contributions may originate from the collective behaviour of the nanoparticles due to differences in their interactions, as observed previously [19].

Switching from physical characterization to *in vivo* characterization to quantify the efficacy of this treatment, the test conditions of the five groups are described in table 1. The first four groups study the effect of field amplitude, while group 5 is a control group with no iron oxide nanoparticles injected, but a field applied. The last three columns also contain the maximum temperature achieved, the normalized rate of heat dosage deposited and the total normalized heat dosage applied. Conventionally, it is expected that the higher heat dosage should generate the larger temperature change (and therefore greater efficacy). However, as the mechanism for how nanoparticle generated heat damages tumor cells is unknown and since the dissipation of nanoparticle delivered heat is also not well characterized, this is too simplistic of a viewpoint. Instead, it appears from these data that the maximum temperature occurs with the largest dosage rate, which occurs with the largest field amplitude and the shortest on time. At first glance, this appears to make sense, if only one physiological response of the mouse is considered. In any endothermic animal, there exist responses to regulate body temperature—either by expanding blood vessels (thermal washout) or by shivering and contraction of blood vessels close to the skin to generate/conserves heat internally. The former process will definitely be a factor in removing convective heat that is generated locally from the iron oxide nanoparticles. Because this is a dynamic process, the faster heat can be deposited into the local area, the greater the temperature change before the physiological response can remove it. However, other physiological responses, such as damage to the blood vessel from heat (at higher temperatures of 46–48 °C), may restrict or even stop such blood flow, creating a higher than expected heating situation, thereby limiting the applicability of this simple view. For this reason, the physical characterization alone is insufficient to determine efficacy;

Table 1. Conditions of *in vivo* mouse trials. The variation in time on is required to prevent unnecessary mortality in the mice.

Group	Amplitude (Oe)	Time On (s)	Particle dose (mg of Fe)	Total heat dose (J g ⁻¹ tumor)	Heat dosage rate (J s ⁻¹ g ⁻¹ tumor)	Maximum temperature (°C)
1	400	900 ± 0	722 ± 50	702.50 ± 0.91	0.780	37.13 ± 1.27
2	550	1002 ± 164	845 ± 183	905.98 ± 137.37	0.904	45.27 ± 2.93
3	550	926 ± 100	436 ± 67	412.19 ± 43.05	0.445	46.80 ± 2.48
4	700	699 ± 276	976 ± 236	669.63 ± 256.51	0.958	51.16 ± 2.40
5	550	1200 ± 0	N/A	N/A	N/A	40.12 ± 2.31

physiological responses must be considered and *in vivo* studies performed in order to truly determine the efficacy of a treatment.

4. Conclusions

The saturation magnetization, particle structure and interparticle interactions all affect the SAR. However, each contributes in different ways and with different magnitudes, and may even be in competition with each other. The biological response in our preliminary studies correlates with the measured intratumoral temperature and thermal dose (time and temperature), leading these nanoparticles to appear to have a ‘global’ therapeutic effect, similar to that of conventional hyperthermia. Finally, the physiological effects (e.g. dynamic heat transport mechanisms) which normally have a major influence on the efficacy of conventional hyperthermia treatment, may not have the same role in nanoparticle hyperthermia. This is likely due to the fact that the heat source for nanoparticle hyperthermia is internal rather than external for conventional hyperthermia and that the cellular targets for nanoparticle hyperthermia may well be different. Further work is necessary to understand the mechanisms of heat damage and heat dissipation in mammals.

Acknowledgments

This work is supported by the US Army Medical Research and Materiel Command under Contract No W81XWH-04-C-0142. The views, opinions and/or findings contained in the report are those of the author(s) and should not be construed as an official Department of the Army position, policy or decision unless so designated by other documentation. This work utilized facilities supported in part by the National Science Foundation under Agreement No DMR-0454672.

References

- [1] Overgaard J 1985 *Hyperthermic Oncology* vol 2, ed J Overgaard (London: Taylor and Francis) pp 8–9
- [2] Streffer C and van Beuningen D 1987 *Hyperthermia and the Therapy of Malignant Tumors* ed J Streffer (Berlin: Springer) pp 24–70
- [3] Zaffaroni N, Fiorentini G and De Giorgi U 2001 *Eur. J. Surg. Oncol.* **27** 340
- [4] Hildebrandt B *et al* 2002 *Crit. Rev. Oncol. Hematol.* **43** 33
- [5] Moroz P, Jones S K and Gray B N 2002 *J. Surg. Oncol.* **80** 149
- [6] Moroz P, Jones S K and Gray B N 2002 *Int. J. Hyperthermia* **18** 267
- [7] Jeffrey S *et al* 1999 *Arch. Surg.* **134** 1064
- [8] Izzo F, Barnett C C and Curley S A 2001 *Adv. Surg.* **35** 225
- [9] DeNardo S J, DeNardo G L, Natarajan A, Miers L A, Foreman A R, Gruettner C, Adamson G N and Ivkov R 2007 *J. Nucl. Med.* **48** 437
- [10] Dewhirst M W, Jones E, Vujaskovic T, Li C and Prosnitz L 2003 *Cancer Medicine* ed D Kufe *et al* (Hamilton, Ontario, Canada, BC: Decker) pp 623–6
- [11] van der Zee J 2002 *Ann. Oncol.* **13** 1173
- [12] DeNardo S J, DeNardo G L, Miers L A, Natarajan A, Foreman A R, Gruettner C, Adamson G N and Ivkov R 2005 *Clin. Cancer Res.* **11** 7087s
- [13] Hoopes P J *et al* 2007 *Proc. SPIE* **6440** 6440K
- [14] Gruettner C, Mueller K, Teller J, Westphal F, Foreman A and Ivkov R 2007 *J. Magn. Magn. Mater.* **311** 181
- [15] Barker J G, Glinka C J, Moyer J J, Kim M H, Drews A R and Agamalian M 2005 *J. Appl. Cryst.* **38** 1004
- [16] Kline S R 2006 *J. Appl. Cryst.* **39** 895
- [17] Ivkov R, DeNardo S J, Daum W, Foreman A R, Goldstein R C, Nemkov V S and DeNardo G L 2005 *Clin. Cancer Res.* **11** 7094S
- [18] Galant C, Amiel C, Wintgens V and Sebille B 2002 *Langmuir* **18** 9687
- [19] Dennis C L, Jackson A J, Borchers J A, Ivkov R, Foreman A R, Goernitz E, Lau J W and Gruettner C 2008 *J. Appl. Phys.* **103** 07A319